ACS Catalysis

Research Article

pubs.acs.org/acscatalysis

Steam Reforming of Ethanol on Ni/CeO_2: Reaction Pathway and Interaction between Ni and the CeO_2 Support

Wenqian Xu,[†] Zongyuan Liu,[†] Aaron C. Johnston-Peck,[‡] Sanjaya D. Senanayake,[†] Gong Zhou,[†] Dario Stacchiola,[†] Eric A. Stach,[‡] and José A. Rodriguez*[,†]

[†]Chemistry Department and [‡]Center for Functional Nanomaterials, Brookhaven National Laboratory, Upton, New York 11973, United States

ABSTRACT: The steam reforming of ethanol on a Ni-based CeO_2-supported catalyst was studied using in situ X-ray diffraction (XRD), operando diffuse reflectance infrared Fourier transform spectroscopy (DRIFTS), and mass spectroscopy (MS) with a focus on the structural characterization of the catalysts, chemical identification of the reaction pathway, and understanding of the interaction between Ni and the CeO_2 support. Ethoxy, acetate, carbonate, and hydroxyl species are identified by DRIFTS as surface intermediates that appear during the reaction process. The oxidation of ethoxy to acetate and the decomposition of acetate are two key steps in the steam reforming process. The CeO_2 support facilitates the oxidation of ethoxy to acetate below 350 °C. Above 350 °C, the Ni metal catalyzes dissociation of the C−C bond in acetate to form carbonate and methyl, something that the CeO_2 support is not able to do. The Ce(III) sites produced by the reduction of ceria in ethanol help to dissociate water forming the surface hydroxyl groups, which react with the methyl groups to produce CO_2 and inhibited the methyl groups' progress to CH_4. Post-reaction transmission electron microscopy (TEM) images of the Ni/CeO_2 catalyst reveal two types of carbon configurations: encapsulating carbon and filamentous carbon. A water-rich atmosphere favors formation of carbon filaments, which do not deactivate the catalyst.

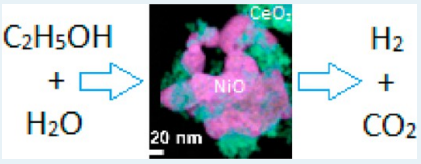

KEYWORDS: *ethanol, steam reforming, nickel, hydrogen production, ceria*

INTRODUCTION

Steam reforming of ethanol ($C_2H_5OH + 3\ H_2O \rightarrow 6\ H_2 + 2\ CO_2$) is of great interests to the chemical industry and fuel cell applications as it provides a route to obtain hydrogen from a renewable and environmentally friendly energy source.[1,2] The reforming process has a complex series of mechanistic steps that involve multiple reactions, and is often accompanied by parallel side reactions that produce undesirable products such as CH_4, C_2H_4, CO, and amorphous carbon, depending on the reaction conditions, such as temperature and the ethanol/steam ratio, as well as the nature of the catalysts.[1,3−7] The reaction schemes proposed in the literature[1−5,8,9] can be summarized as follows: ethanol adsorbed on the catalyst surface may undergo decomposition to CH_4 and CO (eq 1), dehydrogenation to acetaldehyde (eq 2), or dehydration to ethylene (eq 3).

$$C_2H_5OH \rightarrow CH_4 + CO + H_2 \quad (1)$$

$$C_2H_5OH \rightarrow CH_3CHO + H_2 \quad (2)$$

$$C_2H_5OH \rightarrow C_2H_4 + H_2O \quad (3)$$

The acetaldehyde further decomposes to form CH_4 and CO (eq 4) or undergoes steam reforming to CO and H_2 (eq 5).

$$CH_3CHO \rightarrow CH_4 + CO \quad (4)$$

$$CH_3CHO + H_2O \rightarrow 2CO + 3H_2 \quad (5)$$

Methane formed in eq 1 or eq 4 can undergo steam reforming to CO and H_2 (eq 6), or dehydrogenate to carbon and H_2 (eq 7).

$$CH_4 + H_2O \rightleftarrows CO + 3H_2 \quad (6)$$

$$CH_4 \rightarrow C + 2H_2 \quad (7)$$

CO formed in eq 1, eq 4, and eq 6 can either be oxidized to CO_2 through the water gas shift reaction (eq 8), or form carbon through the Boudouard reaction (eq 9).

$$CO + H_2O \rightleftarrows CO_2 + H_2 \quad (8)$$

$$2CO \rightleftarrows C + CO_2 \quad (9)$$

The ethylene from ethanol dehydration can easily polymerize and form coke (eq 10),

$$nC_2H_4 \rightarrow \text{polymers} \rightarrow C \quad (10)$$

which is a third route contributing to carbon formation besides eq 7 and eq 9.[10]

The above proposed reaction scheme is mainly based on chemical analysis of final products during temperature-programmed desorption (TPD) of ethanol or temperature-programmed reaction under steam reforming conditions,[1,4,5] therefore provides little insights regarding the surface species and their transformations during reaction. Recently, surface-sensitive spectroscopic methods such as diffuse reflectance infrared Fourier transform spectroscopy have been routinely used to fill this gap.[7,11−29] Noronha's group studied a series of

Received: February 5, 2013
Revised: March 25, 2013
Published: April 1, 2013

metal/metal oxide catalysts, including Pt/CeO_2,[16] Pd/CeO_2,[17] Pt/ZrO_2,[20] $Pt/CeZrO_2$,[20,23] Co/CeO_2,[17,22] and Ni/La_2O_3.[24] The evolution of surface adsorbates on these catalysts was more or less the same. Ethanol molecules dissociatively adsorb as ethoxy species (CH_3CH_2O-), which further dehydrogenate to acetaldehydes (CH_3CHO-) and acetyls (CH_3CO-). The acetaldehydes and acetyls will be oxidized to acetates (CH_3COO-) that will undergo further oxidation and C−C bond cracking to form carbonates ($-CO_3$). Ozkan's group extensively studied cobalt-based catalysts[14,15,26] and found that the high oxygen mobility of ceria improved catalytic stability and activity when this oxide was doped into a zirconia support.[15]

In this study, we investigate the behavior of a Ni/CeO_2 catalyst for ethanol steam reforming. Ni-based catalysts, owing to nickel's capability for cleaving C−C bonds,[30] have shown good activity and great potential for improved selectivity for the steam reforming reaction in previous studies.[3,31−46] Besides, Ni is a much less expensive choice than the noble metals, like Rh and Ru, which also present good activity in steam reforming.[47] One drawback in the performance of Ni-based catalysts is their vulnerability to carbon deposition.[6,33] In this study, we applied in situ powder X-ray diffraction (XRD) and diffuse reflectance infrared Fourier transform spectroscopy (DRIFTS) to investigate changes in the catalyst structure and the surface speciation during reaction. Transmission electron microscopy (TEM) images were taken for post-reaction samples to examine the morphology of carbon deposition and its relationship with the catalytic activity.

EXPERIMENTAL SECTION

Synthesis. Ni/CeO_2 was prepared by an incipient wetness impregnation method by mixing commercial nickel nitrate and cerium oxide to achieve 20 mol % Ni loading. The sample was dried and calcined at 500 °C in air. Characterization by powder XRD showed that the as-prepared sample contained 8.5 wt % NiO and 91.5 wt % CeO_2, from which the calculated mole ratio of Ni to Ce is 0.21 to 1. The average crystal size estimated with XRD was 8 nm for CeO_2 and 12 nm for NiO.

XRD. Temperature-programmed reduction (TPR) and steam reforming experiments in conjunction with XRD and a residual gas analyzer (RGA) were performed at beamline X7B (λ = 0.3196 Å) of the National Synchrotron Light Source (NSLS) at Brookhaven National Laboratory (BNL). Ni/CeO_2 was studied in three water-free reducing environments (5% H_2 in He, 5% CO in He, and 8% ethanol vapor carried in He) and also under steam reforming conditions as a function of temperature and varying ratios of ethanol to steam (EtOH/H_2O). The generation of the saturated ethanol vapor or water vapor was achieved by passing He through a bubbler filled with pure ethanol or deionized water. The gas flow rate used in this study, 10 cc/min, was sufficiently low to guarantee that the gases passing through the bubblers reached a vapor saturated state. At 25 °C, the saturated vapor pressure was 0.08 bar for ethanol and 0.03 bar for water. The target EtOH/H_2O ratio was achieved by mixing the two vapor gases with an adjustable flow rate for each.

The reaction cell and other parts of the gas flow system have been described in detail elsewhere.[48] Powder samples of 2−3 mg were loaded into a silica capillary (0.9 mm ID, 1.0 mm OD) mounted in the flow cell system. A Perkin-Elmer Amorphous Silicon Detector was used to collect two-dimensional transmission diffraction data, which were subsequently processed with the program Fit2D[49] to obtain XRD profiles (Intensity versus 2θ). Lattice parameters and phase quantities were analyzed by Rietveld Refinement using the program GSAS.[50,51]

DRIFTS. DRIFTS data were collected on Ni/CeO_2, a commercial NiO powder sample and the pure CeO_2 support under steam reforming conditions using a Bruker Equinox 55 FTIR spectrometer equipped with a modified Harrick Praying Mantis DRIFT cell connected to a gas flow system similar to the one used in XRD experiments. Details of the instrument can be found in ref 52. The EtOH/H_2O ratio was kept at 1/8. Stepwise heating and cooling with an incremental of 50 °C up to 400 °C were applied. Temperature was held for 1 h at each step. The composition of the outflow gas was analyzed with a RGA device.

TEM. High resolution TEM images of the as-prepared sample and the samples after reaction experiments were taken at 200 kV using a JEOL JEM 2100F instrument. Sample powders were dispersed as a suspension in deionized water, sonicated for 60 s, and introduced dropwise onto a Holey-C grid and allowed to dry before imaging. Electron energy loss spectroscopy (EELS) and energy disperse X-ray spectroscopy (EDS) chemical maps were acquired on a Hitachi 2700C operated at 200 kV using convergence semi-angles of 23 and 28 mrad, respectively.

RESULTS

1. Interaction of Ni/CeO_2 with Pure EtOH Vapor. *1.1. XRD.* Ni/CeO_2 was heated under a current of ethanol/He from 25 to 400 °C at a rate of 10 °C/min, and then kept at 400 °C for half an hour. Figure 1 shows the time sequence of the XRD profiles covering the 2θ range from 6° to 13°. The NiO phase present in the as-prepared sample is intact till 350 °C, at

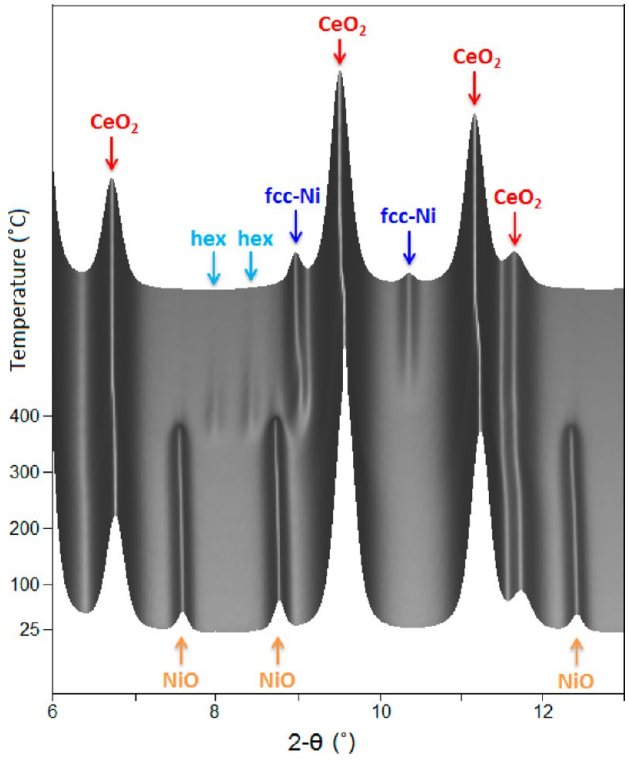

Figure 1. In situ XRD data of Ni/CeO_2 being reduced in pure EtOH vapor. Peaks from the CeO_2 support, the NiO, the fcc-Ni, and the hexagonal intermediate phase (hex) are marked.

dx.doi.org/10.1021/cs4000969 | ACS Catal. 2013, 3, 975−984

which temperature it starts to be reduced to an intermediate hexagonal phase that further transforms into an fcc-Ni (face-centered cubic) phase. The intermediate phase can be either Ni_3C[53] or a hexagonal polymorph of Ni metal,[54] both candidates exhibit similar XRD signatures. The existence of hexagonal Ni has been debated for a long time[54,55] and the most recent study suggests a solid solution series exists between Ni_3C and hexagonal Ni.[56] In this study, formation of the intermediate phase is favored in a carbon-rich environment, including pure EtOH vapor and 5% CO, but not in 5% H_2 or in the steam reforming condition, which implies the intermediate is probably a carbide phase. Quantification of the three Ni-related phases as a function of temperature is plotted in the upper panel of Figure 2. The percentage of Ni in the form of

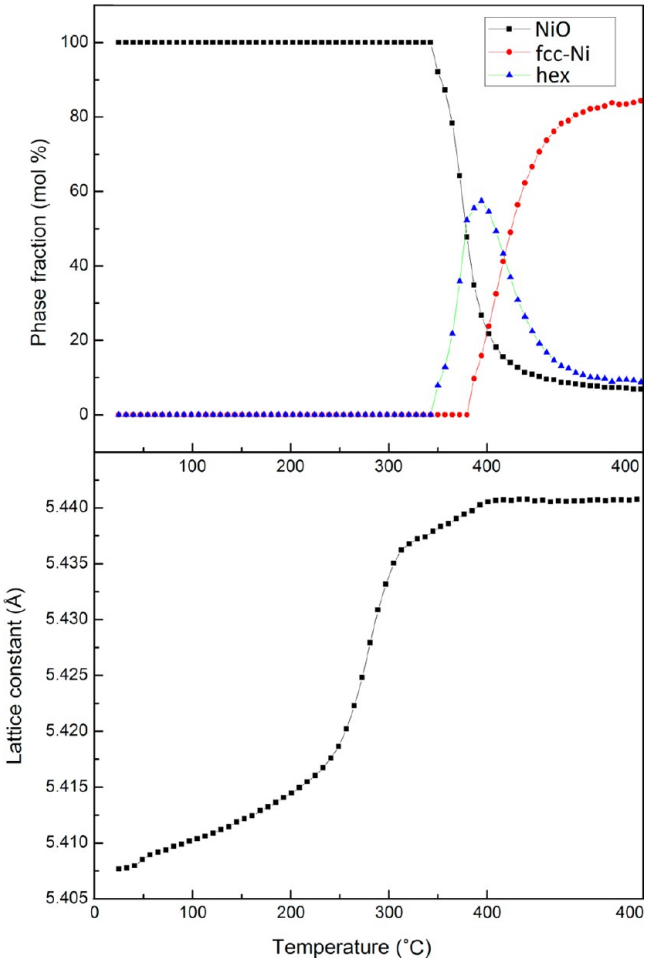

Figure 2. Phase evolution of NiO to metallic Ni (the upper panel) and the change of lattice constant of CeO_2 (the lower panel) during the TPR of Ni/CeO_2 in pure EtOH vapor.

the hexagonal phase reaches a maximum of 60% at 400 °C. The hexagonal phase does not last long before transforming to fcc-Ni. The fcc-Ni appears at 380 °C and dominates at the end of the experiment. In fact, the intermediate phase is metastable under the reaction condition as further study shows it is not possible to avoid the transformation to the fcc-Ni phase even at 350 °C (not shown).

The lower panel in Figure 2 shows the lattice expansion of the CeO_2 support with respect to temperature. It is clear the lattice expansion rate experiences a sharp increase from 230 to 300 °C. This non-thermal expansion is regarded as evidence of partial reduction of Ce(IV) to Ce(III) with removal of oxygen atoms from the crystal structure.[48] A similar phenomenon has been found for pure CeO_2[38,57] and for systems of metals supported on CeO_2.[58] It is a characteristic feature of ceria, but the magnitude of the reduction of this oxide is affected by the presence of a second oxide or metals on its surface.[38,48,57]

1.2. DRIFTS. Figure 3 shows infrared spectra recorded while exposing the as-prepared Ni/CeO_2 to pure ethanol at different

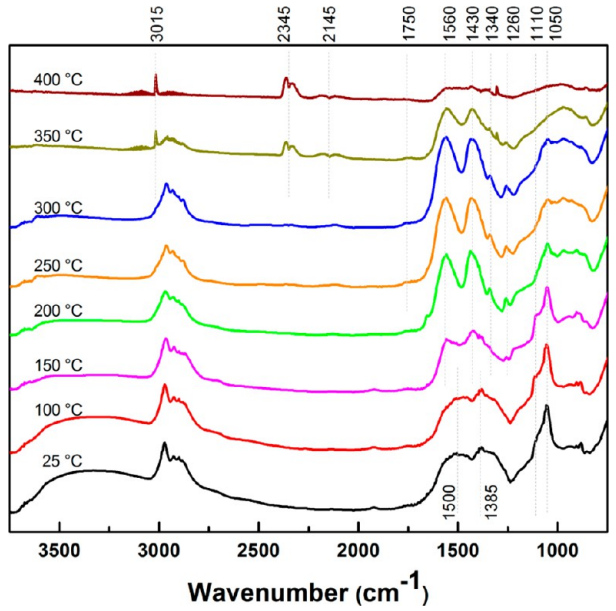

Figure 3. DRIFTS spectra for Ni/CeO_2 at elevating temperatures in pure EtOH vapor environment.

temperatures. At 25 °C, surface-absorbed ethoxy (CH_3CH_2O-) is identified by its characteristic CO bands at 1050 cm^{-1} for bidentate-υ(C−O) and at 1110 cm^{-1} for monodentate-υ(C−O).[12,15] The CH_n stretching bands are found between 2800 and 3000 cm^{-1} ($\upsilon_{as}(CH_3)$ = 2970 cm^{-1}, $\upsilon_{as}(CH_2)$ = 2930 cm^{-1}, $\upsilon_s(CH_3)$ = 2880 cm^{-1}).[11,12] In the COO band region, a broad hump centered at 1500 cm^{-1} that is probably composed of multiple bands and a band at 1385 cm^{-1} are observed. These bands are not well resolved, and their exact identities of are not clear. The line-shape of the bands between 1250 and 1700 cm^{-1} changes from 100 to 150 °C. Two new peaks are identified at 1430 and 1560 cm^{-1}, which can be assigned to the υ_s(COO) band and the υ_{as}(COO) band of acetate (CH_3COO-), respectively.[14,59,60] These two acetate COO bands grow sharply from 150 to 200 °C. The acetate CH_3 bending band also appears at 1340 cm^{-1}. In the meanwhile, the intensities of the ethoxy CO bands at 1110 and 1050 cm^{-1} decrease sharply. These changes indicate dehydrogenation and oxidation of the ethoxy to form the acetate at 200 °C. From 200 to 300 °C, a continuing decrease of the ethoxy CO band intensities with a slight increase of the acetate band intensities can be observed. Also, a very weak peak at 1750 cm^{-1} can be assigned to the υ(CO) band of the CO gas phase. From 300 to 350 °C, the infrared line-shape changes drastically, indicating the appearance of three gas phases: CH_4 (3015 and 1300 cm^{-1}), CO (2145 cm^{-1}), and CO_2 (2345 cm^{-1}), along with decrease of the acetate band intensities and the disappearance of the ethoxy bands. The temperature range correlates with the NiO → Ni transformation seen in XRD (Figure 1).

dx.doi.org/10.1021/cs4000969 | ACS Catal. 2013, 3, 975−984

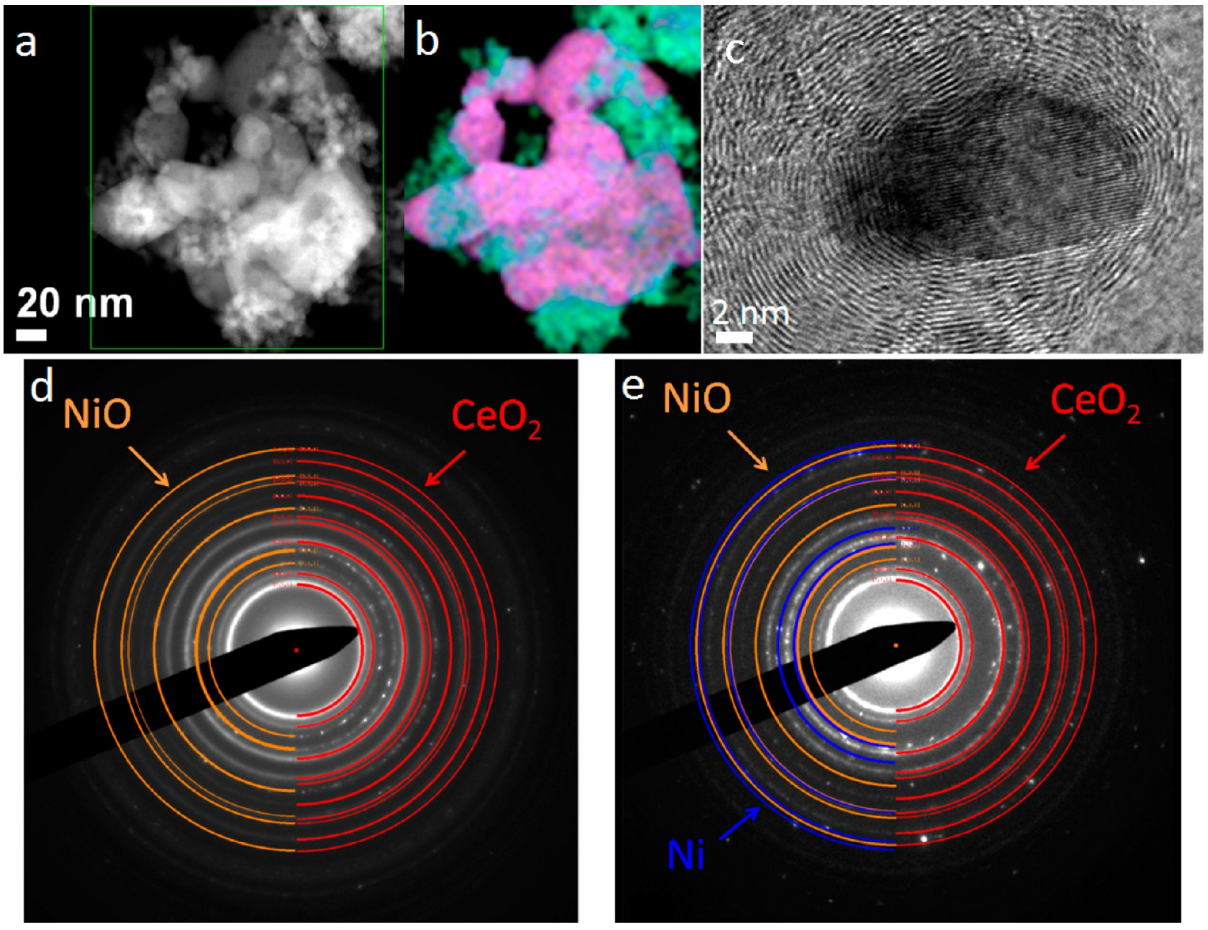

Figure 4. Selected TEM, STEM, and ED images of the as-prepared Ni/CeO_2 (a, b, d) and after reduction in pure EtOH vapor (c, e). The EELS chemical map (b) is color coded to identify and indicate the presence of Ni (red), Ce (blue), and O (green).

1.3. TEM. TEM images of the as-prepared Ni/CeO_2 sample and after reaction in pure EtOH vapor are shown in Figure 4. The as-prepared sample contains spherical CeO_2 particles of an average diameter of 7 nm and irregularly shaped NiO particles of a wide distribution of sizes that extends to ~125−150 nm (XRD indicates an average grain size of 12 nm). Figure 4a and 4b show a scanning transmission electron microscopy (STEM) image of the synthesized sample and the elemental mapping of the same area. The electron diffraction pattern (Figure 4d) consists of diffraction rings of both CeO_2 and NiO. The sample reduced in pure EtOH vapor contains particles encased in layers of graphitic carbon (Figure 4c). EELS (not shown) suggest that the particles encased in graphitic carbon are mainly Ni or NiO. However, small amounts of CeO_x or CeO_2 may be present and remain undetected by our measurements.

2. Ethanol Steam Reforming on Ni/CeO_2. *2.1. XRD.* The performance of Ni/CeO_2 for ethanol steam reforming was studied at different temperatures and different EtOH/H_2O ratios. Figure 5 shows the result of one experiment conducted at a constant EtOH/H_2O ratio of 1/8 with stepwise heating to 300 °C, 350 °C, 400 °C, and 450 °C. In the bottom panel of Figure 5, one can see the simultaneous formation of CO_2 and H_2, as expected for a $C_2H_5OH + 3\ H_2O \rightarrow 6\ H_2 + 2\ CO_2$ reaction. The signal for CH_3 (m/z = 15) could come from the cracking of ethanol or methane in the mass spectrometer. At temperatures above 400 °C, it decreases constantly as a consequence of the consumption of ethanol. Such a behavior implies that no significant amount of methane is formed. The signal m/z = 28, which could be contributed by CO or the cracking of CO_2, increases at 400 °C. The CO/CO_2 ratio in the gas product at 400 °C is estimated to be 1:6, based on the MS data at m/z =28 and m/z = 44 (The CO_2 line). No acetone or acetaldehyde was detected in the RGA. In the upper panel of Figure 5, we summarize results of in situ XRD data for this set of experiments. Rietveld refinement indicates that the NiO phase is directly reduced to the fcc-Ni phase at 350 °C without forming the hexagonal phase as seen in the pure EtOH conditions (Figure 1). As Ni forms at 350 °C, the catalyst is activated and both H_2 and CO_2 are produced (Figure 5 lower panel). Note that the fraction of metallic Ni increases from 0 to 24% during the stay at 350 °C, while the H_2 production peaks at the beginning of the NiO reduction then decreases with time. So it is the initial reduction that occurs at the surface of NiO particles that creates the active metal sites. After that, the continuous growth of metallic Ni shown in XRD comes from the bulk reduction of the NiO crystallites, which does not contribute to activity. Instead, the surface Ni sites could be contaminated with carbon. At 400 °C, the amount of Ni increases to 50% initially, and to 58% after 9 h holding at this temperature. The activity initially increases, and then remains stable for the rest of time at 400 °C. At 450 °C, over 85% of NiO is reduced. Despite an initial boost of activity, the sample tube was soon clogged by carbon, which caused a drop in pressure of all the gas components as illustrated in the mass spectra data (Figure 5 lower panel). The deactivation process

dx.doi.org/10.1021/cs4000969 | *ACS Catal.* 2013, 3, 975−984

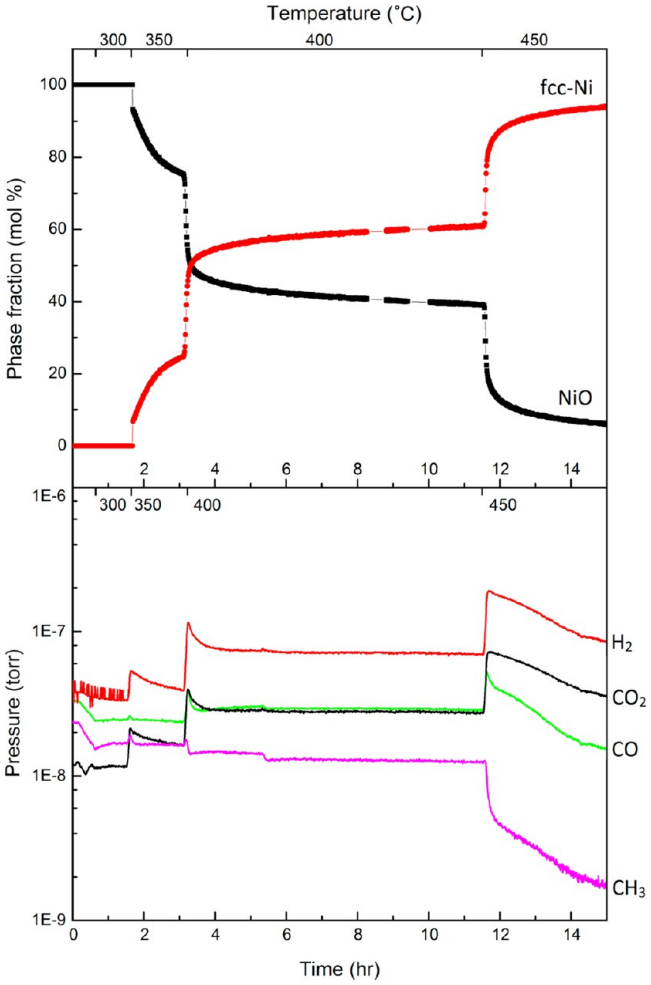

Figure 5. Phase evolution of NiO to metallic Ni (the upper panel) and the mass spectroscopic data of the residual gas (the lower panel) plotted with time and temperature for the steam reforming experiment with the EtOH/H_2O ratio at 1/8.

was reversible. The catalyst was reactivated once the deposited carbon was removed by reaction with O_2.

To study the effect of different EtOH/H_2O ratios on the activity and stability of the catalyst, a different set of experiments was performed. The sample was heated in the same way as in the previous measurement to 400 °C, and kept at this temperature while the EtOH/H_2O ratio was changed. Increasing the EtOH/H_2O ratio from 1/8 to 1/4 slightly increased the production of H_2 and CO_2, but lead to a much higher level of unconverted EtOH in the residual gas. The production of methane did not increase and the reduction of NiO to Ni was not affected by changing the EtOH/H_2O ratio.

2.2. DRIFTS. In situ IR spectra collected for the as-prepared Ni/CeO_2 under ethanol steam reforming conditions (EtOH/H_2O = 1/8) are stack-plotted in Figure 6. The initial sample contains adsorbed water that contributes to a broad hump at 3000 to 3600 cm^{-1} and an OH scissoring band at 1650 cm^{-1}.[15,61] Also identified are the CH_n stretching bands in the region from 2800 to 3000 cm^{-1}, the ethoxy CO bands at 1110 and 1050 cm^{-1},[12,15] and the acetate υ_{as}(COO) band at 1550 cm^{-1}.[14,59,60] The ethoxy bands are of lower intensity than those in Figure 3 because of the lower concentration of EtOH in the gas feed. A second difference from Figure 3 is the formation of acetate on the sample surface at room temperature (RT). At

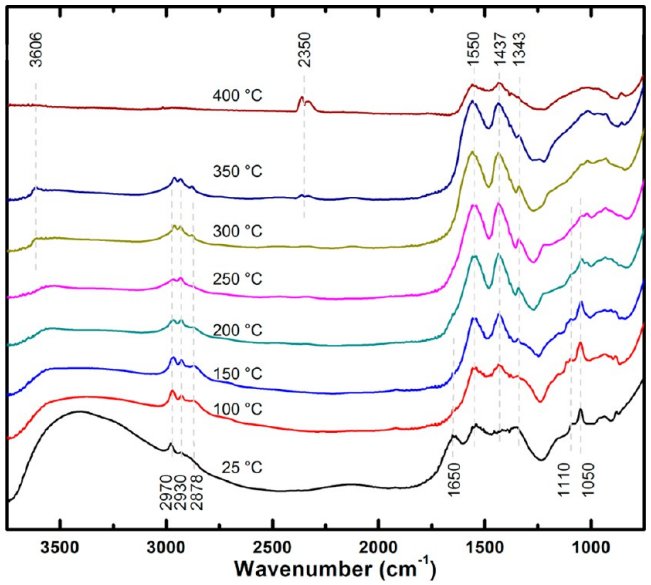

Figure 6. DRIFTS spectra for Ni/CeO_2 at elevating temperatures under steam reforming conditions.

100 °C, the water-related bands diminish. More bands characteristic of the acetate appear, including the symmetric COO stretching band υ_s(COO) at 1437 cm^{-1} and the CH_3 bending band at 1343 cm^{-1}. From 150 to 200 °C, the ethoxy-related bands largely decrease in intensity, while the acetate-related band intensities increase. This transition is also observed at the same temperature in the experiment with pure EtOH (Figure 3). The ethoxy CO bands at 1110 cm^{-1} and 1050 cm^{-1} disappear at 300 °C. From 300 to 350 °C, the CH_3 bending band of the acetate at 1343 cm^{-1} slightly decreases in intensity, which probably indicates the decomposition of the acetate to carbonate. The COO stretching bands of acetates at 1550 cm^{-1} and 1437 cm^{-1} do not obviously decrease in intensity because they are also present in carbonate species with varying frequencies (1534−1568 cm^{-1} and 1430 cm^{-1}).[11,12,62] At 350 °C, CO_2 (centered at 2350 cm^{-1}) is observed in the IR spectrum (Figure 6) and also in the mass spectrum (bottom of Figure 5). At 400 °C, the acetates/carbonates vigorously decompose to form CO_2, shown as a substantial drop of the COO bands (1550 and 1437 cm^{-1}) and a great increase of the CO_2 band intensity. The CH_3 bending band from the acetate (1343 cm^{-1}) and the CH stretching bands (2800−3000 cm^{-1}) disappear. An OH bending band at 3606 cm^{-1} also disappears, which indicates that the hydroxyls are rapidly consumed at 400 °C. The large change in the line-shape seen in the IR spectra from 300 to 400 °C correlates with the NiO → Ni phase transformation seen by in situ XRD.

Figure 7 shows the IR spectra of the pure NiO under the steam reforming condition (EtOH/H_2O = 1/8). At RT, ethoxy (υ(CO) = 1050 and 1100 cm^{-1}), acetate (υ_{as}(COO) = 1550 cm^{-1}, υ_s(COO) = 1415 cm^{-1}, δ(CH3) = 1338 cm^{-1}) and possibly carbonate (bidentate υ_{as}(OCO) = 1562, υ_s(OCO) = 1415) species are present. Water bands (3000 to 3600 cm^{-1}) are not as strong as those in Figure 6, because NiO does not adsorb as much water as CeO_2 does. The ethoxy CO bands decrease in intensity as temperature increases, but still remain prominent at 350 °C. While in the case of Ni/CeO_2, the ethoxy species are completely oxidized to acetate by 300 °C (Figure 6). The acetate-related bands, υ_s(COO) at 1415 cm^{-1} and

dx.doi.org/10.1021/cs4000969 | ACS Catal. 2013, 3, 975−984

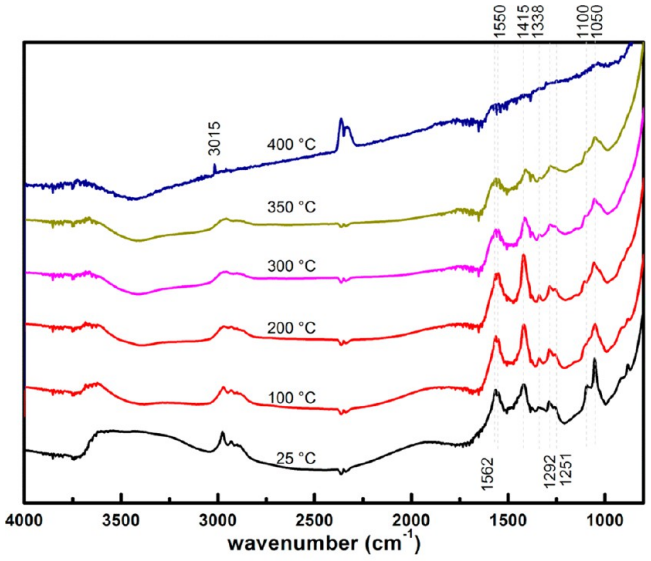

Figure 7. DRIFTS spectra for NiO at elevating temperatures under the steam reforming condition.

δ(CH3) at 1338 cm^{-1}, increase in intensity from RT to 200 °C as some ethoxies are oxidized to acetates, then decrease in intensity from 200 to 350 °C. At 400 °C, along with the production of H_2 and CO_2, a significant amount of methane is released, evidenced by the CH_4 gas band at 3015 cm^{-1}. The methane is probably formed by decomposition of the remaining ethoxy species not oxidized to acetates. It is clear that the CeO_2 support in the Ni/CeO_2 sample helps to completely oxidize the ethoxy species at low temperatures and thus avoids the generation of methane at 400 °C. XRD data (not shown) also confirmed partial reduction of NiO to Ni at 350 to 400 °C.

In the case where only CeO_2 is present in the steam reforming environment, the resulting DRIFTS spectra are shown in Figure 8. Ethoxy and acetate are also observed at 25 °C. Increasing the temperature to 300 °C oxidizes the ethoxy to acetate. At 400 °C, the acetate along with the CH_n bands in the region of 2800−3000 cm^{-1} persists with no formation of CO_2 or CH_4 observed in DRIFTS; the OH groups on CeO_2 indicated by the OH bending band at 3624 cm^{-1} also stays. It is clear that CeO_2 by itself cannot effectively decompose acetate and that the Ni interplay is critical for the efficient steam reforming of ethanol. Comparing the IR results in Figures 3, 6, 7, and 8, one can reach interesting conclusions about the role of each component of the Ni/CeO_2 catalyst in the reaction. Ni is mainly responsible for cleaving C−C bonds of acetates or ethoxies, while the CeO_2 support, other than dispersing NiO particles, has two functions: (1) facilitate the oxidation of ethoxies to acetates; and (2) generate surface OH groups that promote the production of H_2 and CO_2 while inhibiting the formation of CH_4.

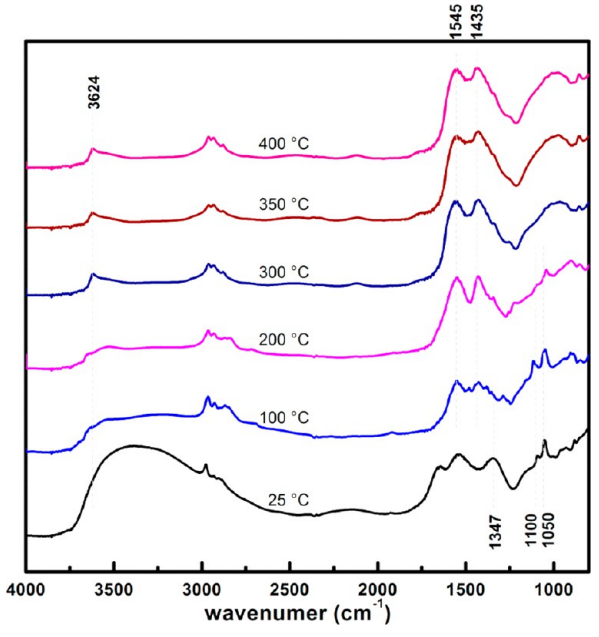

Figure 8. DRIFTS spectra for CeO_2 at elevating temperatures under the steam reforming condition.

2.3. TEM. TEM images recorded after performing ethanol steam reforming on a Ni/CeO_2 sample are shown in Figure 9. As shown in Figure 4, the catalyst exposed to pure EtOH contains Ni/NiO particles completely encapsulated in layers of graphitic carbon. In the sample after steam reforming, particles are mostly supported on carbon fibers. Some of the larger particles appear on the tip on the carbon fiber, indicating that they may have catalyzed the growth of the fiber (Figure 9b).[63] Further elemental analysis shows the particles on the tip contain only Ni without Ce (Figure 9c, d, and e). The fact that the carbon fibers are not present in the sample reduced in pure EtOH indicates the importance of H_2O for its mode of growth.[64] Filamentous carbon has been documented in previous studies on ethanol steam reforming using Ni[33,65] or Co,[66] and may not deactivate the catalyst as the encapsulating carbon does.[33] Our results support this argument, as the sample presenting the carbon fibers did not deactivate after staying 10 h at 400 °C. In fact, TEM data obtained of samples undergoing long reaction times (Figure 10) show well dispersed small particles (<2 nm) that have become embedded or supported on the carbon fibers. The arrows in Figure 10 point to 1−2 nm size particles. STEM EELS indicates particles like these are most frequently NiO_x but CeO_x particles were identified as well.

DISCUSSION

1. Active Phase. On the basis of the results from both the DRIFTS and the XRD experiments, it is clear that Ni metal in close contact with CeO_2 is the active phase catalyzing the steam reforming reaction. On Ni/CeO_2, acetates start to break down at 350 °C (Figure 6), when NiO was reduced to Ni as seen in XRD (Figure 5). On pure CeO_2 without Ni, the formed acetates do not decompose or transform to other species up to 400 °C (Figure 8). Without the CeO_2 support, acetates can still be decomposed by Ni, but with a significant production of CH_4 because of the insufficient supply of OH (Figure 7). Therefore, neither Ni nor CeO_2 can effectively transform the acetate to the desired gas products, CO_2 and H_2, by itself. The interaction of Ni and CeO_2 in the catalyst is important for the proper functioning of the catalyst and, as we will discuss below, it is likely that Ni and ceria work in a cooperative way catalyzing different parts of the reaction.

2. Reaction Intermediates. The reaction intermediates observed in our DRIFTS experiments are ethoxy, acetate, carbonate, and hydroxyl. The same species were also observed in previous studies on Co systems[14,15,22,26] and Pt systems.[12,16,20,23] On the surface of Ni/CeO_2, NiO and CeO_2, both ethoxy and acetate are observed in all three cases at RT in

dx.doi.org/10.1021/cs4000969 | ACS Catal. 2013, 3, 975−984

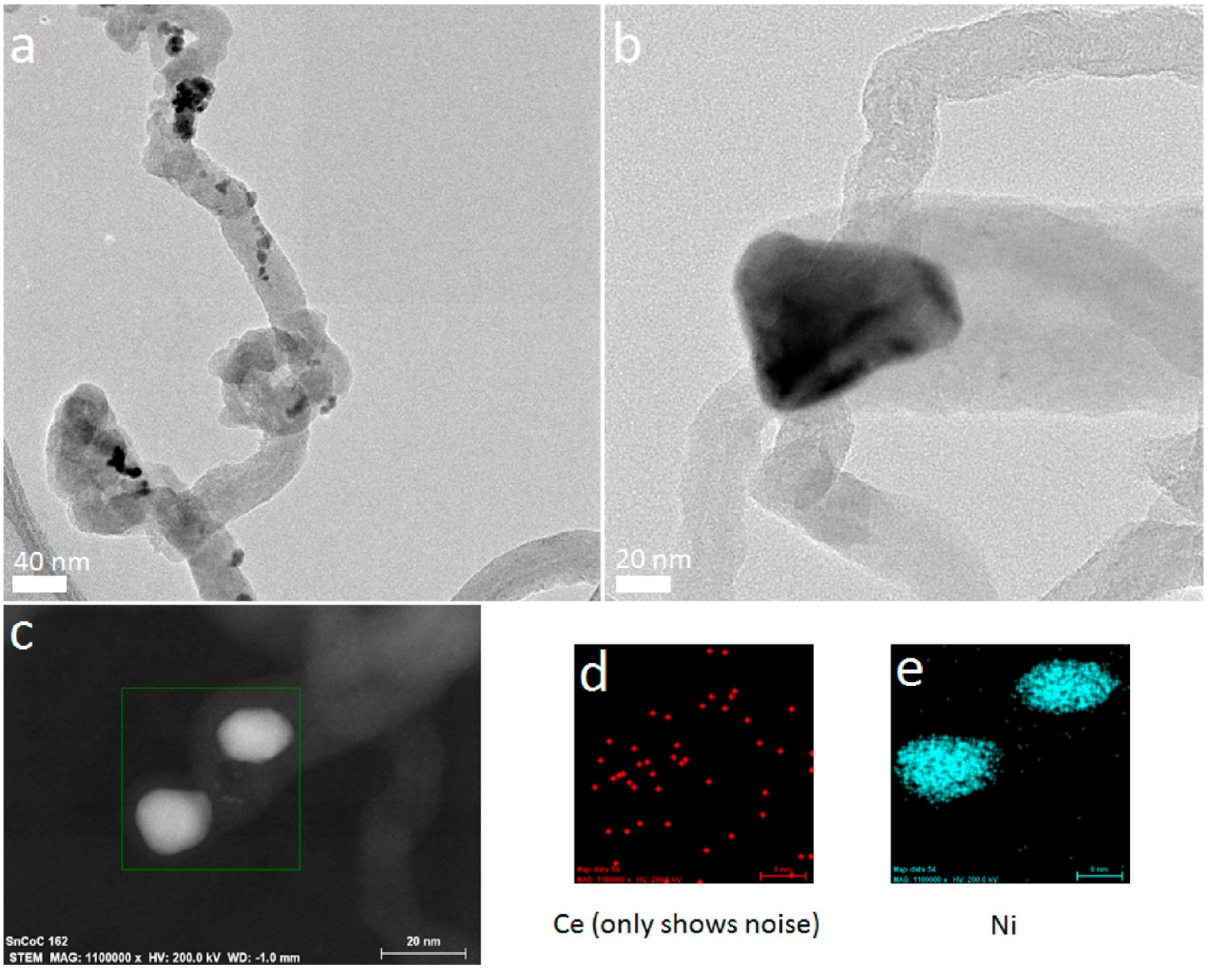

Figure 9. Selected TEM and STEM collected after performing the steam reforming of ethanol on a Ni/CeO_2 catalyst showing the carbon fibers.

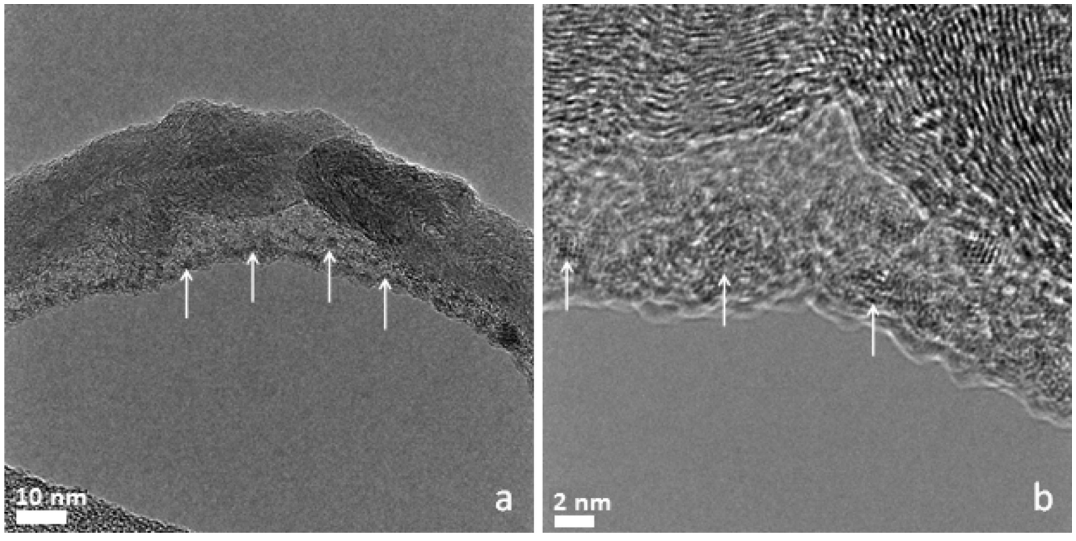

Figure 10. TEM images of Ni/CeO_2 catalyst after the steam reforming reaction showing embedding of small (<2 nm) particles (white arrows) in fibrous carbon (a) and higher magnification images of particles (b).

the steam reforming atmosphere, while the relative abundance of the two species varies. On NiO, the ethoxy bands are more prominent; on CeO_2 or Ni/CeO_2, the acetate bands are more intense. As temperature increases to 300 °C, all ethoxies are oxidized to acetate on CeO_2 or on Ni/CeO_2, while only a portion of the ethoxies are oxidized on NiO. Clearly, the CeO_2 support helps oxidize the ethoxies. The formation of acetate on CeO_2 at RT has also been observed in previous research,[11,15] which has been attributed to the high oxygen mobility in CeO_2.[15] A thoroughly prereduced CeO_2 may not be able to form acetate at RT.[11,22] Besides being affected by the CeO_2 support, the formation of acetate at RT is also facilitated by the

dx.doi.org/10.1021/cs4000969 | ACS Catal. 2013, 3, 975−984

presence of water vapor in the feed. Acetate was seen on Ni/CeO_2 at RT under a water and ethanol mixture (Figure 6), but not in the pure EtOH vapor environment (Figure 3). The conversion from ethoxy to acetate, apparently a one-step transition in DRIFTS, is often considered to involve multiple steps: ethoxy dehydrogenates to form adsorbed acetaldehyde, which dehydrogenates again to acetyl, which is finally oxidized to acetate. Identification of acetyl is difficult because its υ(C−O) band is close to the OH scissoring band at 1650 cm^{-1}. Acetaldehyde, on the contrary, should be easily identified based on its υ(C═O) band at 1700 to 1720 cm^{-1}. However, adsorbed acetaldehyde is not observed in our DRIFTS experiments. Similarly, the adsorbed acetaldehyde was not indicated in the in situ DRIFTS spectra of Co/CeO_2[15] or Pt/CeO_2[20] during ethanol TPD, although acetaldehyde was reported in the TPD profiles from both studies.[15,20] The absence of the adsorbed acetaldehyde is probably because (1) the transition from acetaldehyde to acetate is very rapid, and (2) the unreacted acetaldehyde tends to desorb from the surface.[6,26]

The decomposition of acetate occurs above 300 °C. This step of reaction involves C−C bond breaking and formation of carbonate and methyl groups, and is facilitated when Ni is present. In DRIFTS, the COO bands of acetate and carbonate are rather close in position; this transition is mainly identified by the weakening of the CH_3 bending band (1347 cm^{-1}) that is unique to the acetate. Above 350 °C, the carbonate dissociates to CO_2, and H_2 is produced. This coincides with the temperature at which metallic Ni forms as shown in the XRD data (Figure 3 and 4). Without Ni, acetate does not decompose on the surface of CeO_2 (Figure 7), thus no production of H_2 and CO_2. It is important to mention that the presence of Ni adatoms alone is not enough to produce the decomposition of the acetate intermediate. In a set of experiments we generated Ni on the ceria surface and investigated the reforming of ethanol at different temperatures finding that the reaction proceeded well only at temperatures above 300 °C. Thus, there are activation barriers associated with the acetate → carbonate → CO_2 gas transformations that can be overcome only at elevated temperatures and in the presence of Ni.

It is worth noting that acetaldehyde decomposition (not via acetate) could still be a key route for hydrogen production, and is not excluded by the results of the current study, even though acetaldehyde is not observed in DRIFTS. Nonetheless, H_2 formation through acetate should at least be regarded as a secondary reaction route, since the $-CH_3$ group in acetate ultimately goes to H_2 instead of CH_4. Both the acetaldehyde decomposition pathway and the acetate decomposition pathway have been identified in a previous study,[29] where a PtNi/Al_2O_3 catalyst was able to continue catalyzing the ethanol steam reforming reaction via the acetate route after the acetaldehyde decomposition pathway was deactivated.

3. Role of CeO_2. In the Ni/CeO_2 catalysts, the role of CeO_2 is unique beyond just serving as a material to disperse the Ni. CeO_2 has the ability to release and regain oxygen as the oxidation state of Ce changes between +3 and +4. It acts as an oxygen tank when used as the support of a catalyst, readily able to donate and harvest oxygen in redox processes. In the current study of steam reforming of ethanol, CeO_2 facilitates the oxidation of ethoxy to acetate. This is important because the DRIFTS results show the unoxidized ethoxies remaining on the catalyst surface at 300 °C will favor the decomposition route to form methane at higher temperature (Figure 3 and Figure 7). Furthermore, the Ce(III) sites produced by the reduction of CeO_2 in ethanol help to dissociate water forming the surface OH groups that can react with methyl groups to form CO_2 rather than methane. Therefore, the CeO_2 support has a role of inhibiting the formation of CH_4 and allowing for the production of H_2. In addition, from previous studies of valence photoemission[38,57] and recent theoretical calculations,[67] it is known that strong metal−support interactions between Ni and ceria perturb the electronic and chemical properties of Ni adatoms reducing their ability to break C−O bonds. Thus, the Ni↔ceria interactions substantially decrease the CO methanation activity of Ni;[57] an important factor to take into account when dealing with the steam reforming of ethanol on Ni/CeO_2.

4. Mechanism for C Deactivation and the Formation of C Fibers. In the generation of the CO_2 and H_2 gas products and in the formation of the C fibers, the Ni and the ceria work in a cooperative way. Above we have described possible routes for the transformation of $C_2H_xO_y$ into CO_2/H_2 by interaction with Ni and ceria centers. The mechanism for the formation of the C fibers also involves both phases of the catalyst. The general routes for carbon formation have been described in eq 7, eq 9, and eq 10 in the Introduction section. Since eq 10 involves ethylene which is not observed in this study, methane dehydrogenation (eq 7) and the Boudouard reaction (eq 9) are the two probable routes for the carbon formation on the Ni/CeO_2 catalyst. Considering the DRIFTS experimental results and the above discussion on the reaction intermediates and the strong Ni↔ceria interactions, it is reasonable to pinpoint the methyl groups from the decomposition of acetates or ethoxies as the major precursors for carbon deposition on the surface of the catalyst. As discussed above, the water content in the input gas has a major impact on the final gas phase evolved from the methyl groups, and it may also affect the formations of carbon. In a water-less environment as in the experiment of Ni/CeO_2 reduction in pure EtOH vapor, the methyl dehydrogenation is favored; thus layers of carbon can be accumulated in a relatively short time that encapsulated the whole particle (Figure 4). While in a water-rich environment, the methyl dehydrogenation is inhibited, and the carbon accumulation rate on the Ni surface is slow; on the other hand, water may clean part of the surface C by oxidizing it to CO or CO_2. A combination of these two effects can keep one side of the Ni surface always exposed while carbon is being slowly generated and deposited on the other side of the particle, therefore producing the fiber structures seen in Figure 9 and 10.

CONCLUSIONS

We have studied the steam reforming reaction of ethanol over a Ni/CeO_2 catalyst. We have utilized a combination of in situ (DRIFTS and XRD) and ex situ (TEM) techniques to elucidate the role of the catalyst under reaction conditions, identify intermediates, and ascertain the reaction pathways that lead to the production of H_2 and also to the deactivation of the catalyst. The active components of the catalyst under steam reforming condition include metallic Ni and Ce^{3+}. Ni helps in the adsorption of the ethanol and in the cleavage of its C−C bond, while Ce^{3+} facilitates the decomposition of water with the subsequent generation of OH groups which are essential for reacting with C_xH and C_yO_zH and produce CO_2 and H_2. The reaction pathway leads to CO_2 and H_2 predominantly via the formation of ethoxy, acetate, and carbonate surface species. TEM images reveal both encapsulating carbon and filamentous carbon on the surface of the catalyst. A water-rich atmosphere

dx.doi.org/10.1021/cs4000969 | ACS Catal. 2013, 3, 975−984

favors formation of the filamentous carbon, which does not lead to the deactivation of the catalyst.

AUTHOR INFORMATION

Corresponding Author

*E-mail: rodrigez@bnl.gov.

Notes

The authors declare no competing financial interest.

ACKNOWLEDGMENTS

The work carried out at the BNL Chemistry Department, CFN and the NSLS was financed by the U.S. Department of Energy (DOE), Office of Basic Energy Science (DE-AC02-98CH10086).

REFERENCES

(1) Haryanto, A.; Fernando, S.; Murali, N.; Adhikari, S. *Energy Fuels* **2005**, *19*, 2098.
(2) Demirbas, A. *Prog. Energy Combust. Sci.* **2007**, *33*, 1.
(3) Fatsikostas, A. N.; Verykios, X. E. *J. Catal.* **2004**, *225*, 439.
(4) Vaidya, P. D.; Rodrigues, A. E. *Chem. Eng. J.* **2006**, *117*, 39.
(5) Ni, M.; Leung, D. Y. C.; Leung, M. K. H. *Int. J. Hydrogen Energy* **2007**, *32*, 3238.
(6) Mattos, L. V.; Jacobs, G.; Davis, B. H.; Noronha, F. B. *Chem. Rev.* **2012**, *112*, 4094.
(7) Idriss, H. *Platinum Met. Rev.* **2004**, *48*, 105.
(8) Benito, M.; Sanz, J. L.; Isabel, R.; Padilla, R.; Arjona, R.; Daza, L. *J. Power Sources* **2005**, *151*, 11.
(9) Bshish, A.; Yakoob, Z.; Narayanan, B.; Ramakrishnan, R.; Ebshish, A. *Chem. Pap.* **2011**, *65*, 251.
(10) Trimm, D. L. *Catal. Today* **1997**, *37*, 233.
(11) Yee, A.; Morrison, S. J.; Idriss, H. *J. Catal.* **1999**, *186*, 279.
(12) Yee, A.; Morrison, S. J.; Idriss, H. *J. Catal.* **2000**, *191*, 30.
(13) Llorca, J.; de la Piscina, P. R.; Dalmon, J. A.; Homs, N. *Chem. Mater.* **2004**, *16*, 3573.
(14) Song, H.; Zhang, L. Z.; Watson, R. B.; Braden, D.; Ozkan, U. S. *Catal. Today* **2007**, *129*, 346.
(15) Song, H.; Ozkan, U. S. *J. Catal.* **2009**, *261*, 66.
(16) Mattos, L. V.; Noronha, E. *J. Catal.* **2005**, *233*, 453.
(17) Mattos, L. V.; Noronha, F. B. *J. Power Sources* **2005**, *152*, 50.
(18) Erdohelyi, A.; Rasko, J.; Kecskes, T.; Toth, M.; Domok, M.; Baan, K. *Catal. Today* **2006**, *116*, 367.
(19) de Lima, S. M.; da Cruz, I. O.; Jacobs, G.; Davis, B. H.; Mattos, L. V.; Noronha, F. B. *J. Catal.* **2008**, *257*, 356.
(20) de Lima, S. M.; Silva, A. M.; da Cruz, I. O.; Jacobs, G.; Davis, B. H.; Mattos, L. V.; Noronha, F. B. *Catal. Today* **2008**, *138*, 162.
(21) de Lima, S. M.; Colman, R. C.; Jacobs, G.; Davis, B. H.; Souza, K. R.; de Lima, A. F. F.; Appel, L. G.; Mattos, L. V.; Noronha, F. B. *Catal. Today* **2009**, *146*, 110.
(22) de Lima, S. M.; da Silva, A. M.; da Costa, L. O. O.; Graham, U. M.; Jacobs, G.; Davis, B. H.; Mattos, L. V.; Noronha, F. B. *J. Catal.* **2009**, *268*, 268.
(23) de Lima, S. M.; Silva, A. M.; Graham, U. M.; Jacobs, G.; Davis, B. H.; Mattos, L. V.; Noronha, F. B. *Appl. Catal., A* **2009**, *352*, 95.
(24) de Lima, S. M.; da Silva, A. M.; da Costa, L. O. O.; Assaf, J. M.; Jacobs, G.; Davis, B. H.; Mattos, L. V.; Noronha, F. B. *Appl. Catal., A* **2010**, *377*, 181.
(25) de Lima, S. M.; da Silva, A. M.; Jacobs, G.; Davis, B. H.; Mattos, L. V.; Noronha, F. B. *Appl. Catal., B* **2010**, *96*, 387.
(26) Soykal, I. I.; Sohn, H.; Ozkan, U. S. *ACS Catal.* **2012**, *2*, 2335.
(27) Panagiotopoulou, P.; Verykios, X. E. *Int. J. Hydrogen Energy* **2012**, *37*, 16333.
(28) Akdim, O.; Cai, W. J.; Fierro, V.; Provendier, H.; Van Veen, A.; Shen, W. J.; Mirodatos, C. *Top. Catal.* **2008**, *51*, 22.
(29) Sanchez-Sanchez, M. C.; Yerga, R. M. N.; Kondarides, D. I.; Verykios, X. E.; Fierro, J. L. G. *J. Phys. Chem. A* **2010**, *114*, 3873.
(30) Murakami, M.; Matsuda, T. *Chem. Commun.* **2011**, *47*, 1100.
(31) Fatsikostas, A. N.; Kondarides, D. I.; Verykios, X. E. *Catal. Today* **2002**, *75*, 145.
(32) Sanchez-Sanchez, M. C.; Navarro, R. M.; Fierro, J. L. G. *Int. J. Hydrogen Energy* **2007**, *32*, 1462.
(33) Alberton, A. L.; Souza, M.; Schmal, M. *Catal. Today* **2007**, *123*, 257.
(34) Coleman, L. J. I.; Epling, W.; Hudgins, R. R.; Croiset, E. *Appl. Catal., A* **2009**, *363*, 52.
(35) Frusteri, F.; Freni, S.; Chiodo, V.; Spadaro, L.; Di Blasi, O.; Bonura, G.; Cavallaro, S. *Appl. Catal., A* **2004**, *270*, 1.
(36) Yang, Y.; Ma, J. X.; Wu, F. *Int. J. Hydrogen Energy* **2006**, *31*, 877.
(37) Youn, M. H.; Seo, J. G.; Cho, K. M.; Park, S.; Park, D. R.; Jung, J. C.; Song, I. K. *Int. J. Hydrogen Energy* **2008**, *33*, 5052.
(38) Gong, Z.; Barrio, L.; Agnoli, S.; Senanayake, S. D.; Evans, J.; Kubacka, A.; Estrella, M.; Hanson, J. C.; Martiacutenez-Arias, A.; Fernaacutendez-Garciacutea, M.; Rodriguez, J. A. *Angew. Chem., Int. Ed.* **2010**, *49*, 9680.
(39) Jalowiecki-Duhamel, L.; Pirez, C.; Capron, M.; Dumeignil, F.; Payen, E. *Int. J. Hydrogen Energy* **2010**, *35*, 12741.
(40) Muroyama, H.; Nakase, R.; Matsui, T.; Eguchi, K. *Int. J. Hydrogen Energy* **2010**, *35*, 1575.
(41) Li, S. R.; Li, M. S.; Zhang, C. X.; Wang, S. P.; Ma, X. B.; Gong, J. L. *Int. J. Hydrogen Energy* **2012**, *37*, 2940.
(42) Profeti, L. P. R.; Habitzheuter, F.; Assaf, E. M. *Quim. Nova* **2012**, *35*, 510.
(43) Rossetti, I.; Biffi, C.; Bianchi, C. L.; Nichele, V.; Signoretto, M.; Menegazzo, F.; Finocchio, E.; Ramis, G.; Di Michele, A. *Appl. Catal., B* **2012**, *117*, 384.
(44) Zhang, C. X.; Zhang, P.; Li, S. R.; Wu, G. W.; Ma, X. B.; Gong, J. L. *Phys. Chem. Chem. Phys.* **2012**, *14*, 3295.
(45) Sun, J.; Wang, Y. G.; Li, J. G.; Xiao, G. L.; Zhang, L. G.; Li, H.; Cheng, Y. L.; Sun, C. W.; Cheng, Z. X.; Dong, Z. C.; Chen, L. Q. *Int. J. Hydrogen Energy* **2010**, *35*, 3087.
(46) Akiyama, M.; Oki, Y.; Nagai, M. *Catal. Today* **2012**, *181*, 4.
(47) Liguras, D. K.; Kondarides, D. I.; Verykios, X. E. *Appl. Catal., B* **2003**, *43*, 345.
(48) Xu, W. Q.; Si, R.; Senanayake, S. D.; Llorca, J.; Idriss, H.; Stacchiola, D.; Hanson, J. C.; Rodriguez, J. A. *J. Catal.* **2012**, *291*, 117.
(49) Hammersley, A. P.; Svensson, S. O.; Hanfland, M.; Fitch, A. N.; Hausermann, D. *High Pressure Res.* **1996**, *14*, 235.
(50) Larson, A. C.; Von Dreele, R. B. *General structure analysis system (GSAS)*; Los Alamos National Laboratory: Los Alamos, NM, 2000.
(51) Toby, B. H. *J. Appl. Crystallogr.* **2001**, *34*, 210.
(52) Marinkovic, N. S.; Wang, Q.; Frenkel, A. I. *J. Synchrotron Radiat.* **2011**, *18*, 447.
(53) Hofer, L. J. E.; Cohn, E. M.; Peebles, W. C. *J. Phys. Colloid Chem.* **1950**, *54*, 1161.
(54) Hemenger, P.; Weik, H. *Acta Crystallogr.* **1965**, *19*, 690.
(55) He, L. *J. Magn. Magn. Mater.* **2010**, *322*, 1991.
(56) Schaefer, Z. L.; Weeber, K. M.; Misra, R.; Schiffer, P.; Schaak, R. E. *Chem. Mater.* **2011**, *23*, 2475.
(57) Senanayake, S. D.; Evans, J.; Agnoli, S.; Barrio, L.; Chen, T. L.; Hrbek, J.; Rodriguez, J. A. *Top. Catal.* **2011**, *54*, 34.
(58) Hurtado-Juan, M. A.; Yeung, C. M. Y.; Tsang, S. C. *Catal. Commun.* **2008**, *9*, 1551.
(59) Li, C.; Sakata, Y.; Arai, T.; Domen, K.; Maruya, K.; Onishi, T. *J. Chem. Soc., Faraday Trans. 1* **1989**, *85*, 929.
(60) Li, C.; Sakata, Y.; Arai, T.; Domen, K.; Maruya, K. I.; Onishi, T. *J. Chem. Soc., Faraday Trans. 1* **1989**, *85*, 1451.
(61) Du, X. Z.; Dong, L.; Li, C.; Liang, Y. Q.; Chen, Y. *Langmuir* **1999**, *15*, 1693.
(62) Vayssilov, G. N.; Mihaylov, M.; St Petkov, P.; Hadjiivanov, K. I.; Neyman, K. M. *J. Phys. Chem. C* **2011**, *115*, 23435.
(63) Helveg, S.; Lopez-Cartes, C.; Sehested, J.; Hansen, P. L.; Clausen, B. S.; Rostrup-Nielsen, J. R.; Abild-Pedersen, F.; Norskov, J. K. *Nature* **2004**, *427*, 426.
(64) Hata, K.; Futaba, D. N.; Mizuno, K.; Namai, T.; Yumura, M.; Iijima, S. *Science* **2004**, *306*, 1362.

(65) Zhang, B. C.; Tang, X. L.; Li, Y.; Cai, W. J.; Xu, Y. D.; Shen, W. J. *Catal. Commun.* **2006**, *7*, 367.
(66) Llorca, J.; Homs, N.; Sales, J.; de la Piscina, P. R. *J. Catal.* **2002**, *209*, 306.
(67) Carrasco, J.; Barrio, L.; Liu, P.; Rodriguez, J. A.; Ganduglia-Pirovano, M. V. *J. Phys. Chem. C* **2013**, in press, DOI: 10.1021/jp400430r.